

Calibration of Numerical and Determination of Physical Parameters for the Organic Model System TRIS-NPG

Johann P. Mogeritsch¹, Bernd Böttger², Andreas Ludwig¹

¹Montanuniversitaet Leoben, Department of Metallurgy, Chair for Simulation and Modelling of Metallurgical Processes, 8700 Leoben, Austria,

²access, Intzestraße 5, 52072 Aachen, Germany

¹johann.mogeritsch@unileoben.ac.at, ²b.boettger@access-technology.de,

¹andreas.ludwig@unileoben.ac.at

Abstract— *Studies on the formation of layered peritectic solidification structures have been carried out by using the model system TRIS-NPG (tris[hydroxymethyl]aminomethane - neopen-tylglycol). As such structures are highly affected by thermo-solutal convection, further studies are planned aboard the International Space Station in 2020/21. Since convection is always present on earth, the required process conditions for μg -experiments need to be elaborated by experiments under earth gravity (1g) conditions, also by numerical investigations. In order to do so, not only adequate physical properties are required, but also numerical parameters have to be characterized. Given that there is an insufficient knowledge of corresponding physical properties for the model system, the determination of the required parameters takes place by parameter variation with the aim to match with the obtained experimental results.*

Index Terms— ESA, phase field method, peritectic layered structures, TRIS-NPG.

I. INTRODUCTION

The transparent organic components TRIS-NPG [1] are used by the authors as model system to study the formation of peritectic layered structures close to the range of constitutional undercooling. In-situ observations were performed during direct solidification by employing the Bridgman technique. This enables to study the dynamic of the solid/liquid (s/l) interface and the resulting microstructures [2]-[16]. However, such structures are sensitive to fine concentration fluctuation caused by convection ahead of the solidification front. Since convection is always present on earth, corresponding experiments are going on to be carried out under μg conditions aboard the International Space Station (ISS) in 2020/21. Accompanying numerical investigations are performed to ensure to obtain peritectic layered structures with the selected process conditions in Space. In order to do so the commercial phase field code MICRESS [17] was used. The phase field method [17]-[18] is a mathematical model for solving interfacial problems [19], where the conditions at the interface are substituted by a partial differential equation for the evolution of an auxiliary field, called phase field. It is usually constructed in such a way that the limit of an infinitesimal interface width, the

so-called sharp interface limit, the correct interfacial dynamics are recovered. This approach permits solving the problem without explicit treatment of the boundary conditions at the interface [19]. In addition to the process conditions some specific material values are required for numerical investigations. Furthermore, there is a set of numerical parameters in MICRESS which strongly affect the result of the simulation. Such parameters are essential to determine the phase-field modelling. In the worst case inappropriate numerical parameters can lead to numerical instability and eventually to a hard crash, but even stable looking simulations can give incorrect results.

In this paper we present the conclusion of our investigations to ensure that the numerical parameters don't influence the numerical results. This is a premise for further numerical investigations on peritectic layered structures. Based on the obtained experimental results under 1g conditions, 2-dimension (2D) simulations which neglect thermo-solutal convection were performed in order to determine the required parameters.

II. PROCESS CONDITIONS

A peritectic reaction is characterized by the formation of the peritectic [β] phase from the primary [α] phase and a liquid [L] at the peritectic temperature, T_p , and at the peritectic concentration, C_β [20]. Peritectic layered structures are a special pattern where both phases solidify alternately [21]-[22] under non-stable conditions. The solidification experiment [14] was used as a source to calibrate the parameters. In contrast to peritectic layer structures, in which both phases grow simultaneously, the solidification patterns observed in [14] show the transformation from the primary phase to the peritectic phase in a "short jump". Hereby, the initial primary phase solidifies in a dendritic manner (Fig.1a) until the peritectic phase nucleates at the solid/liquid interface [14]. According to the temperature gradient and the position within the adiabatic gap, the nucleation event took place at 405.05 K which corresponds to an undercooling of the peritectic phase of $T_u = 5.6$ K. Overgrowing the primary phase seaweed-like, the β phase grows with cellular morphology (Fig.1b). This circumstance enables to compare the unique solidification pattern of each phase independently under the same process condi-

tions. Specifically, these were a pulling rate of $V_p = 0.32 \pm 0.01 \mu\text{m/s}$, a temperature gradient of $G_T = 6.5 \pm 0.1 \text{ K/mm}$ within the observation area, and a total observation time of $t = 61,350 \text{ s}$. The micro Bridgman-furnace has been designed in such a way that a rectangular glass tube ($100 \mu\text{m} \times 2000 \mu\text{m}$ inner dimension), filled with the organic compound, was pulled from the hot zone to the cold zone. The tube was illuminated through the adiabatic zone so that the morphology of the s/l interface could be observed using a transmitted light microscope in combination with a black-and-white camera. During solidification, images were recorded all 30 s and stored for further evaluation. Details on compound preparation, sample preparation, as well as on the Bridgman-furnace can be found in [4]-[16]. During the solidification experiment the organic material solidified over a length of $16,366 \pm 50 \mu\text{m}$, departed in $6674 \mu\text{m}$ for the primary phase and $9,692 \mu\text{m}$ for the peritectic phase. Hereby, the growth rate was slightly lower than $0.26 \mu\text{m/s}$ for the primary phase and slightly higher than $0.26 \mu\text{m/s}$ for the peritectic phase.

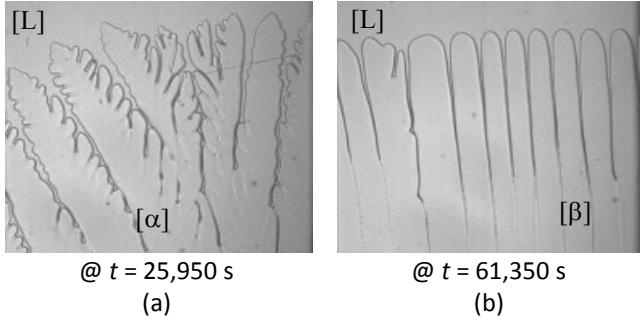


Fig.1: (a) Dendritic solidification pattern for the primary α phase, and (b) cellular growth for the peritectic β phase. The pictures show a width of $1.800 \mu\text{m}$.

III. MATERIALS PARAMETERS AND INITIAL SETTINGS

Reliable thermo-physical parameters are critical for performing phase-field simulations. The organic compounds - especially around the peritectic concentration - were hardly studied [9] and only few data are available, see Table 1.

Table 1: Published properties of TRIS and NPG.

		TRIS	NPG
$\rho @ 298$ [23]	g/cm^3	1.35	0.98
M [24]	g/mol	121.1	104.1
T_m [23]	K	445 – 446	398 – 403
ΔH_m [25]	kJ/mol	3.7 ± 0.2	4.4 ± 0.2
ΔS_m [26]	$\text{J/mol}\cdot\text{K}$	7.12	10.8
ΔV_m [26]	cm^3/mol	6.63	4.86

Investigations by [11] determined the diffusion coefficient for the peritectic region as $D_l = 1.0 \pm 0.5 \cdot 10^{-7} \text{ cm}^2/\text{s}$. For the interface energies there are no reported literature data, therefore values need to be calibrated in the following. The starting point was $\sigma_{s/l} = 1.0 \cdot 10^{-5} \text{ J/cm}^2$ for the liquid/ α phase and liquid/ β phase, respectively. The solid/solid phase transformation was numerical included, but the values for the solid diffusion coefficients D_s were set to

$1.0 \cdot 10^{-12} \text{ cm}^2/\text{s}$. The length of the diffusion profile δ ahead of the s/l interface is given by:

$$\delta = \frac{2 \cdot D_l}{V_p} \quad (1)$$

With the above mentioned values the diffusion length becomes $\delta = 62.5 \mu\text{m}$. MICRESS has a “moving_frame” option which allows for the reduction of the simulation domain to a small part of the Bridgman furnace which follows the solidification front. The movement of the simulation domain is controlled by the distance between the s/l interface and the top of the domain. This distance is set as $200 \mu\text{m}$. Due to the fact that no Thermo-Calc [27] data for the TRIS-NPG system have been found, the phase diagram had to be defined in linear form. It consists of a reference temperature ($T_p = 410.7 \text{ K}$), the slopes of the liquidus and solidus line and the reference points where the slopes cross the reference temperature (Fig.2).

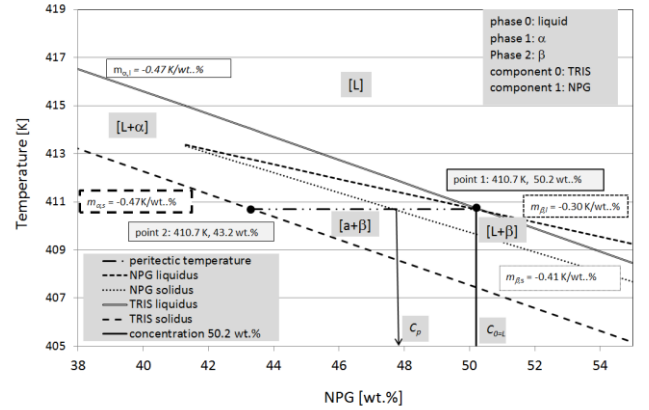


Fig.2: Input data which defines the peritectic region.

The most critical parameters for numerical stability are the grid resolution and the interface mobility. On one hand, the grid size Δx must be selected in such a way to resolve the diffusion profiles, which are related to the diffusion coefficients D_l and the growth velocity V of the interface, and the expected curvature of the occurred interface morphology. In fact, this requires a high resolution obtained by a fine grid size. On the other hand, the interface mobility given by the kinetic coefficient μ must be high enough to allow diffusion-controlled growth. Hence, the simplest way to obtain a stable simulation is to reduce the grid size as small as possible and put the value for the kinetic coefficient as high as possible. But increasing the grid resolution by a factor of 2 will result in a factor of 4-16 for the simulation time concerning a 2-dimensional simulation. For the initial simulation run the kinetic coefficient is set to $\mu = 1 \cdot 10^{-5} \text{ cm}^4/\text{J}\cdot\text{s}$ and the grid size to $\Delta x = 2 \mu\text{m}$. The entropy of fusion S_f is set as $1.9 \text{ J/cm}^3\cdot\text{K}$, as an arbitrary start point, while both pure substances exhibit a higher value. Together with the surface tension $\sigma_{s/l}$ and the critical radius r_c the entropy of fusion defines the necessary undercooling T_u for a growable nucleus, as

$$\Delta T_u = \frac{2}{r_c} \cdot \frac{\sigma}{S_f} \quad (2)$$

The “stabilization” option is selected to neglect the curvature until the grain reaches a sufficient size with a fraction close to 1 within the central cell. Therefore, a “numerical” undercooling is defined by the cell size. According to equation 2 a “numerical” undercooling of $T_{u,n} = 0.05$ K is obtained. Since the experimentally observed undercooling is much higher ($T_u = 5.6$ K), the cell size doesn’t affect the nucleation event. The width of the domain corresponds to only one third of the experimental width. The boundary conditions for the concentration field were chosen as periodic for the east and west side and as fixed concentration ($C = 50.2$ wt.%) for the top. Table 2 summarizes the selected parameters as starting points for the initial 2-dimension numerical investigations.

Table 2: Selected numerical and physical parameter

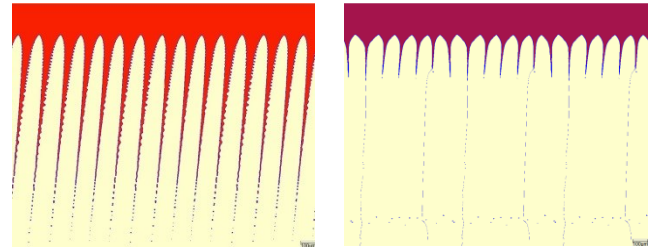
numerical parameters			
domain			
wide	x	cells	333
solidification direction	z	cells	800
cell size	Δx	μm	2
kinetic coefficient	μ	$\text{cm}^4/\text{J}\cdot\text{s}$	$1\cdot 10^{-5}$
phase field	West, East (periodic) Bottom (symmetric) Top (isolated)		
concentration field	West, East (periodic) Bottom (isolated) Top (fixed)		
time step	automatic		
physical parameters			
diffusion coefficient	D_l	m^2/s	$1.0\cdot 10^{-7}$
surface energy	$\sigma_{s/l}$	J/cm^2	$1.0\cdot 10^{-5}$
temperature gradient	G_T	K/cm	65
cooling rate	\dot{T}	K/s	$2.08\cdot 10^{-3}$
concentration	C	wt.%	50.2
simulation time	t_α	s	25,950
	t_β	s	35,400
entropy of fusion	$S_{f\alpha,\beta}$	$\text{J}/\text{cm}^3\cdot\text{K}$	1.9

Both phases are assumed to be anisotropic and cubic. The “1d_far_field” option was selected with a distance of 200 μm ahead of the s/l interface to reduce calculation time. The interfacial stiffness coefficient was put to 0.3 to avoid faceted structure and the anisotropy of the interfacial mobility was set to 0.1. Separate simulations were carried out for each phase, whereby, the initial conditions were, for all simulations, a centered α phase grain at the domain bottom ($600 \mu\text{m} \times 152 \mu\text{m}$). No nucleation was allowed for the investigations of the α phase. In future, nucleation of the β phase will be performed at the α/l interface.

IV. FIRST RESULTS AND FURTHER ADJUSTMENTS

Since the domain was reduced to 1/3 of the original sample size, all numerical results were 3 times mirrored to

obtain the same width as for the solidification experiments Fig. 3 displays the numerical results for the initial parameters. The final solidification morphology for the primary α phase after 25950 s, corresponding to the experimental time, is shown in Fig. 1a. Within this time a solidification length of 8,064 μm was achieved, approximately 20% more than in the experiment. Furthermore, the number of dendrites was twice as high as in the experiment. The result of the peritectic phase is similar (Fig.3b). Again, the solidification length is exceeded by 18% (11,346 μm), and the number of cells was increased by 1.6 times. The distance between the dendrite/cell tips is $\lambda_{l,\alpha} = 125 \mu\text{m}$ for the α phase and $\lambda_{l,\beta} = 111 \mu\text{m}$ for the β phase.



(a) @ 25950 s (b) @ 35400 s

Fig. 3: The microstructure of the (a) α phase and (b) β phase obtained for the initial setting.

The discrepancy in solidification length can be explained by considering the actual solidification rate. While the sample was moved with an average $V_p = 0.267 \mu\text{m}/\text{s}$ during the experiment, the solidification velocity during the primary solidification was only $V_{\alpha,\beta} = 0.26 \mu\text{m}/\text{s}$. Hence, this difference must be taken into account when adjusting the parameters.

A. Validation of the Cell Size

The relationship between cell size Δx and kinetic coefficient μ was checked by comparing the increase of solid fraction as a function of simulation time for varied kinetic coefficients, shown in Fig. 4.

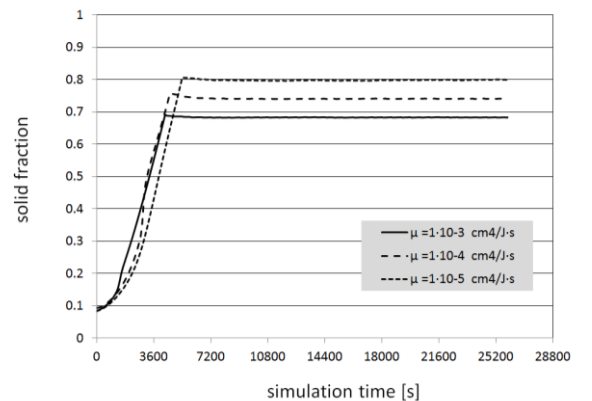


Fig. 4: Amount of solid fraction as function of the simulation time and different kinetic coefficients μ .

The horizontal line indicates action of of the “moving_frame”. As soon as the s/l interface reached the predefined distance of 200 μm , the domain follows the s/l interface. It can be seen that the rise of solid fraction is very

similar for all variations of the kinetic coefficient. It has to be noted, that the final solid fraction differed since the interdendritic melt proportion varies according to the selected kinetic coefficient.

The experimental investigations shows a dendritically solidification morphology for the α phase, whereas, the simulation displays cells. Therefore, further investigations were carried out to define possible ranges for the physical parameters surface energy σ and entropy of fusion S_f as well the numerical parameter kinetic coefficient μ .

B. Estimation of the Surface Energy

A first adjustment was made by adapting the surface energy. As shown in Fig. 5 it is evident that with decreasing surface energy the microstructure changes from cellular to dendritic.

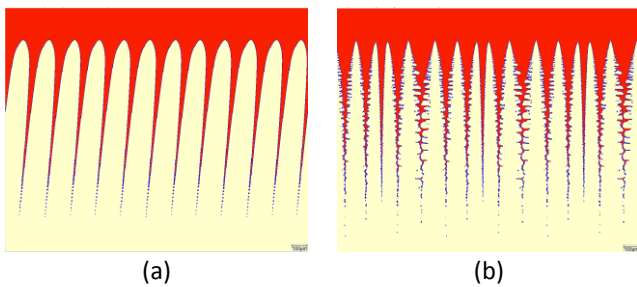


Fig. 5: Microstructure patten for the α phase obtained with a surface energy of (a) $\sigma = 1 \cdot 10^{-4}$ J/cm² and (b) $\sigma = 1 \cdot 10^{-6}$ J/cm². ($\mu = 1 \cdot 10^{-4}$ cm⁴/J·s for both cases)

Several simulations were carried out by varying the surface energy for both phases until the obtained microstructures were close to the experimental results. The results showed that the surface energy had to be reduced to $\sigma = 1 \cdot 10^{-6}$ J/cm² for the primary α phase. For the β phase (Fig. 6), the numerical outcome shows in a slightly higher value, namely $\sigma = 5 \cdot 10^{-5}$ J/cm².

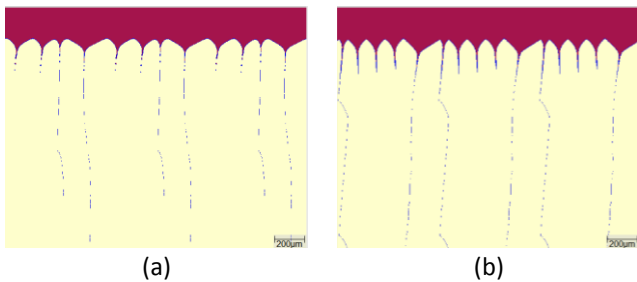


Fig. 6: Cellular growth of the β phase with (a) $\sigma = 5 \cdot 10^{-5}$ J/cm² and (b) $\sigma = 5 \cdot 10^{-6}$ J/cm². ($\mu = 1 \cdot 10^{-4}$ cm⁴/J·s for both cases)

Another general effect that results from decreasing the surface energy was that the cell tips became sharper.

C. Set of the Kinetic Coefficient

As soon as the surface energy magnitude was fixed, the kinetic coefficient was varied. The assessment was done in the same way as for the parameters before, by comparison with the images taken during the solidification experiment.

The results (Fig. 7) show that the originally selected kinetic coefficient lies within a reasonable range and a further enlargement leads to an unstable simulation, shown as blue dots in Fig. 7.a. Furthermore, it should be noted that a reduction of the coefficient leads to a decrease of the number of dendrites/cells (compared the α -phase with 15 dendrites in Fig. 5.b and 9 cells in Fig. 7b).

Based on the obtained results the kinetic coefficient was adapted for both phases to $\mu = 1 \cdot 10^{-4}$ cm⁴/J·s.

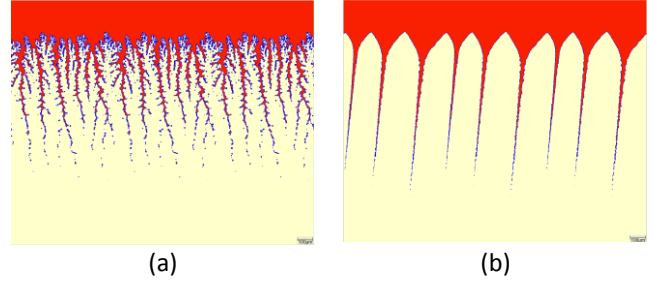


Fig. 7: α phase microstructure with $\sigma = 1 \cdot 10^{-6}$ J/cm² for (a) $\mu = 1 \cdot 10^{-3}$ cm⁴/J·s and (b) $\mu = 1 \cdot 10^{-5}$ cm⁴/J·s.

D. Entropy of Fusion

Unfortunately, the critical nucleus size r_c is unknown, therefore, the entropy can't be calculated by equation 2. Therefore, the entropies of fusion were estimated by comparing different simulations with the existing experimental result as shown in Fig. 8 for the β phase. It's obvious that by increasing the entropy the number of cells increased also.

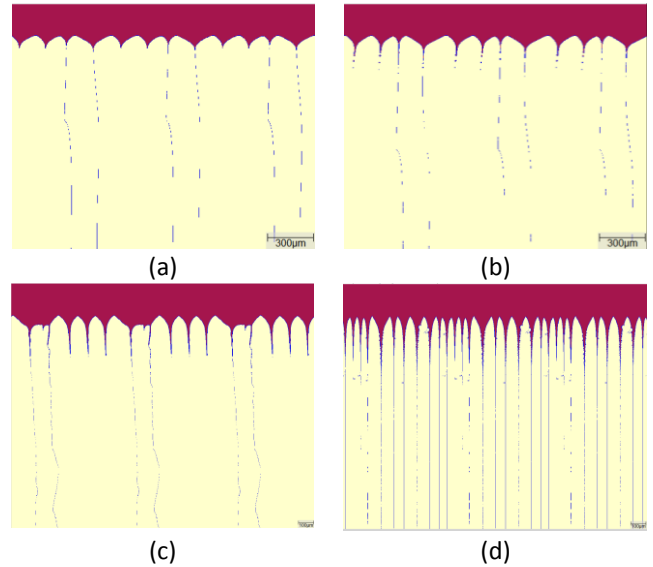


Fig. 8: β phase solification structure obtain with (a) $S_f = 0.5$ J/cm³·K, (b) $S_f = 0.8$ J/cm³·K, (c) $S_f = 1.4$ J/cm³·K, (d) $S_f = 6.0$ J/cm³·K.

The corresponding results for the α phase are shown in Fig. 9. If the entropy is set too high, fine dendrites develop (Fig.9d) or in the opposite case the structure changes from dendrites (Fig. 9.a-d) to cells (not shown). Changing the entropy of fusion essentially balances the effects of curvature and chemical driving force, and thus has similar effects as varying the interfacial energy σ .

The highest possible degree of correlation was achieved for both phases between the experiments and the numerical results for an entropy of fusion of $S_f = 0.5 \text{ J/cm}^3 \cdot \text{K}$.

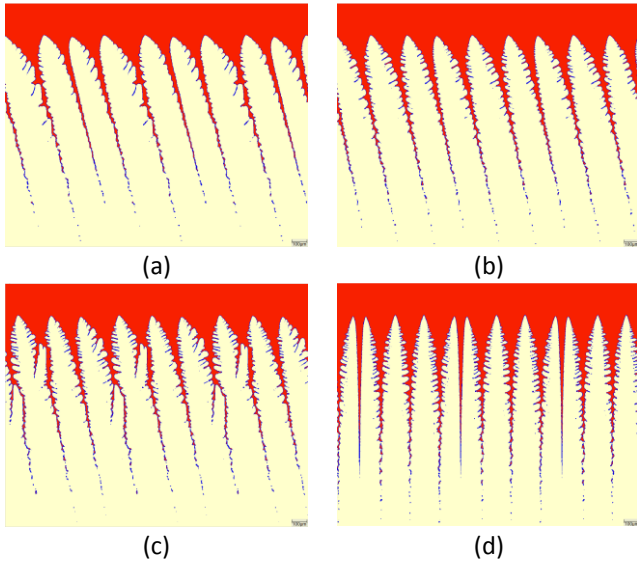


Fig. 9: Solidification pattern for the α phase with (a) $S_f = 0.5 \text{ J/cm}^3 \cdot \text{K}$, (b) $S_f = 0.8 \text{ J/cm}^3 \cdot \text{K}$, (c) $S_f = 1.0 \text{ J/cm}^3 \cdot \text{K}$, (d) $S_f = 1.4 \text{ J/cm}^3 \cdot \text{K}$.

V. RESULTS AND DISCUSSION

As a last step, a fine tuning was carried out. Based on the gained intermediate results, the surface tension and the kinetic mobility were once again varied in the range of a power of ten. The interfacial mobility $\mu(\theta)$ and the stiffness $\sigma^*(\theta)$ were improved in order to adjust the curvature and the formation of the secondary arms. The optimal match as shown in Fig. 10 was found for stiffness factors of $\sigma^*(\theta) = 0.3$ for both phases.

When evaluating the simulations, it should be remembered that the experimental microstructure was formed in the presence of thermo-solutal convection, in contrast to the numerical. Furthermore, the cooling rate in the simulation was adjusted in such a way that the experimental total solidification length could be reproduced numerically. The deviation for the α phase is now 1.3 % and 0.9 % for the second phase. This differences are due to the not exactly matched cooling rate.

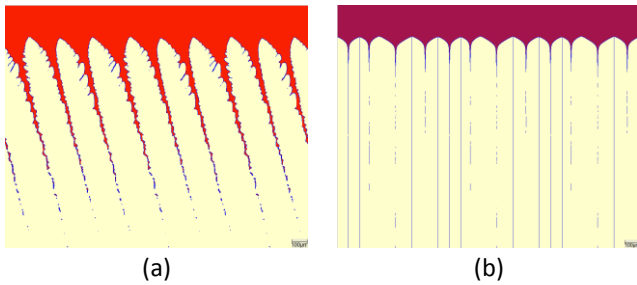


Fig. 10: Simulated microstructure for the (a) α phase with $\sigma = 1 \cdot 10^{-6} \text{ J/cm}^2$, $\mu = 1 \cdot 10^{-4} \text{ cm}^4/\text{J} \cdot \text{s}$ and $S_f = 0.5 \text{ J/cm}^3 \cdot \text{K}$ and the (b) β phase with $\sigma = 5 \cdot 10^{-5} \text{ J/cm}^2$, $\mu = 1 \cdot 10^{-4} \text{ cm}^4/\text{J} \cdot \text{s}$ and $S_f = 0.8 \text{ J/cm}^3 \cdot \text{K}$.

To demonstrate the quality of the matches, an enlarged section of Fig. 1 and Fig. 10 are shown in Fig. 11. For this comparison, the colorful images of the numerical results were converted into grey images.

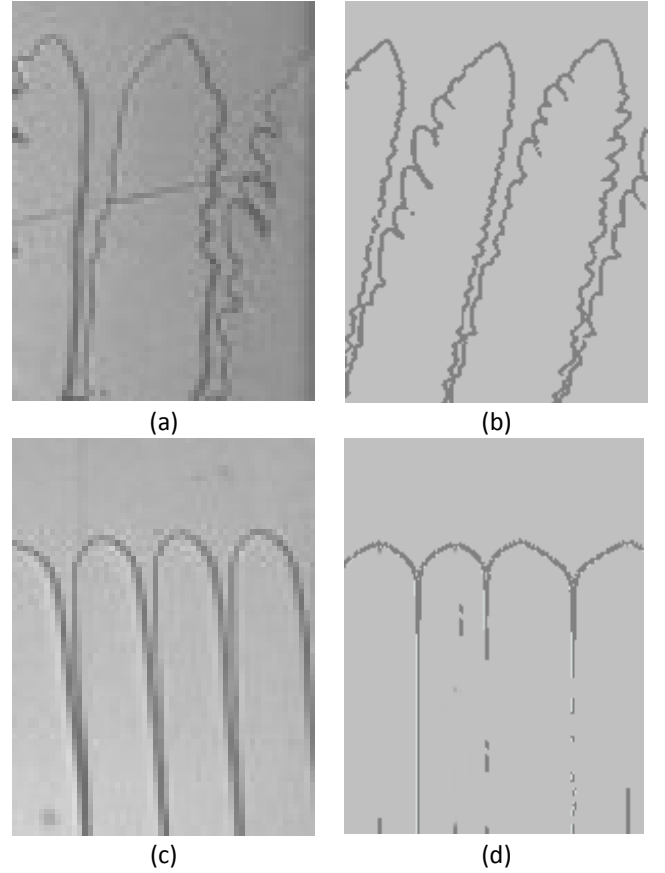


Fig. 11: Comparison of the, (a) experimental and (b) numerical microstructure for the α phase and the (c) experimental and (d) numerical results for the β phase. The widths of the images are $590 \mu\text{m}$.

The finally selected physical and numerical parameters are given in Table 3.

Table 3: Selected numerical and physical parameter

surface energy α phase	$\sigma_{s/l}$	J/cm^2	$1.0 \cdot 10^{-6}$
surface energy β phase	$\sigma_{s/l}$	J/cm^2	$5.0 \cdot 10^{-5}$
cooling rate	\dot{T}	K/s	$1.76 \cdot 10^{-3}$
entropy	$S_{f,\alpha}$	$\text{J/cm}^3 \cdot \text{K}$	0.5
	$S_{f,\beta}$	$\text{J/cm}^3 \cdot \text{K}$	0.8
interfacial stiffness coefficient	$\sigma^*(\theta)$		0.3
interfacial mobility coefficient	$\mu(\theta)\alpha$		0.02
	$\mu(\theta)\beta$		0.01

VI. CONCLUSIONS AND OUTLOOK

For investigations of layered peritectic structures, direct solidification experiments were performed with the organic model system TRIS-NPG. Since these peritectic patterns are

strongly influenced by thermo-solutal convection, further experiments on board the ISS are planned for 2020/21. In order to pre-determine the process conditions under μg -conditions, numerical investigations were performed without taking convection into account. For this purpose the phase-field based software program MICRESS was used. To obtain stable simulations, it was checked whether the selected cell size or the kinetic coefficient had an influence on the numerical results. Due to insufficient published physical data, numerical investigations were carried out to define the physical parameters surface energy and entropy of fusion for the organic compound. The possible range of physical parameters was first narrowed down by a rough variation of the values. Then, a finer tuning and the final adjustment took place via interfacial stiffness and mobility. Based on the gained results, further numerical investigations on peritectic layered structures can now be started to define the process conditions for the μg -experiments aboard the ISS.

ACKNOWLEDGEMENT

This research has been supported by the Austrian Research Promotion Agency (FFG) in the frame of the METTRANS projects and by the European Space Agency (ESA) in the frame of the METCOMP project.

REFERENCES

- [1] M. Barrio, D.O. Lopez, J.L. Tamarit, P. Negrier., and Y. Haget, "Degree of miscibility between non-isomorphous plastic phases: Binary system NPG (Neopentylglycol)- TRIS (tris[hydroxymethyl]aminomethane)," *Mater Chem.* Vol. 5, no. 3, pp. 431-439, March 1995.
- [2] J. Mogeritsch, A. Ludwig, S. Eck, M. Grasser, and B. McKay, "Stability investigations of a binary organic alloy system with a peritectic phase diagram," *Scripta Mater.* Vol. 60, pp. 882-885, May 2009.
- [3] J. Mogeritsch, S. Eck, M. Grasser, and A. Ludwig, "In-situ observation of solidification in an organic peritectic alloy system," *Mater. Sci. Forum*, vol. 649, pp. 159-64, 2010.
- [4] A. Ludwig, J. Mogeritsch., and M. Grasser, "In-situ observation of unsteady peritectic growth modes," *Trans. Indian Inst. Met.*, vol. 62, pp. 433- 436, August 2009.
- [5] A. Ludwig, and J. Mogeritsch, "In-situ observation of coupled peritectic growth," *Solidif. Sci. Technol. Proc. John Hunt Int. Symp.*, pp. 233-242, 2011.
- [6] J. Mogeritsch, and A. Ludwig, "In-situ observation of coupled growth morphologies in organic peritectics," *IOP Conf. Ser. Mater Sci. Eng.* 7, pp. 12028, Mai 2011.
- [7] J. Mogeritsch, and A. Ludwig, "Microstructure formation in the two phase region of the binary peritectic organic system TRIS-NPG," TMS Annual Meeting Symposium, Materials Res Microgravity, Orlando, Florida, USA, pp. 48-56, 2012.
- [8] J. Mogeritsch, "Investigation on peritectic solidification using a transparent organic system," Ph.D. Thesis, Montanuniversitaet Leoben, AUT, 2012 available at <http://smmp.unileoben.ac.at>
- [9] A. Ludwig, and J. Mogeritsch, "Recurring instability of cellular growth in a near peritectic transparent NPG-TRIS alloy system," *Mater Sci. Forum*, pp. 317-22, 2014.
- [10] J. Mogeritsch, and A. Ludwig, "In-situ observation of the dynamic of peritectic coupled growth using the binary organic system TRIS-NPG," *IOP Conf. Ser. Mater Sci. Eng.*, vol. 84, pp. 12055, 2015.
- [11] A. Ludwig, J. Mogeritsch, "Compact seaweed growth of peritectic phase on confined, flat pro-peritectic dendrites," *Journal of Crystal Growth* 455, pp. 99-104, September 2016.
- [12] A. Ludwig, J. Mogeritsch., T. Pfeifer, "In-situ observation of coupled peritectic growth in a binary organic model alloy," *Acta. Mat.*, vol. 126, pp. 329-335, March 2017.
- [13] J.P. Mogeritsch, A. Ludwig, "Investigation on peritectic layered structures by using the binary organic components TRIS-NPG as model substances for metal-like solidification," *Crimson Publishers, Res. Dev. Mater. Sci.*, vol. 4(1), pp. 1-3, February 2018
- [14] J.P. Mogeritsch, and A. Ludwig, "Investigation on the binary organic components TRIS-NPG as suitable model substances for metal-like solidification," 7th Int. Conf. Solidification and Gravity, pp. 330-335, September 2018.
- [15] J.P. Mogeritsch, T. Pfeifer, M. Stefan-Kharicha, and A. Ludwig "Investigation on the liquid flow ahead of the solidification front during the formation of peritectic layered solidification structures," 7th Int. Conf. Solidification and Gravity, pp. 319-324, September 2018
- [16] J.P. Mogeritsch, and A. Ludwig, "In-situ observation of growth morphologies in organic peritectics," *Int. Jour. Trend Res. Dev. Special Issue*, pp. 174-179, December 2018.
- [17] <https://web.micress.de/>
- [18] Eiken J, Böttger B, Steinbach I (2006) Multiphase-field approach for multicomponent alloys with extrapolation scheme for numerical application. *Phys Rev E* 73:066122.
- [19] W.J. Boettinger, J.A. Warren, C. Beckermann, and A. Karma, "Phase-field simulation of solidification," *Annual Review of Materials Research.*, vol. 32: pp. 163–194, 2002.
- [20] W. Kurz, and R. Trivedi, "Banded solidification microstructures," *Metallurgical and Materials Transactions A*, vol. 27, pp. 625-634, 1996.
- [21] T.S. Lo, S. Dobler, M. Plapp, A. Karma, and W. Kurz, "Two phase microstructure selection in peritectic solidification: from island banding to coupled growth," *Acta Mater.* 51, pp. 599–611, 2003.
- [22] S. Dobler, T.S. Lo, M. Plapp, A. Karma, and W. Kurz, "Peritectic coupled growth," *Acta Mater.* 52, pp. 2795–2808, 2004.
- [23] <http://www.merck.de>
- [24] <http://en.wikipedia.org/wiki/Tris>
- [25] M. Barrio, D.O. Lopez, J.L. Tamarit, P. Negrier and Y .Haget, J. "Molecular interactions and packing in molecular alloys between nonisomorphous plastic phases," *Solid State Chem.* 124, pp. 29-38, 1996.
- [26] J.Ll. Tamarit, B. Legendre, J. M. Buisine, "Thermodynamic study of some neopentane derivated by thermobarometric analysis," *Mol. Cryst. Liq. Cryst.* 250, pp. 347-358, 1994.
- [27] <https://www.thermocalc.com/>